journal

J. Am. Ceram. Soc., 90 [6] 1792–1797 (2007)
DOI: 10.1111/j.1551-2916.2007.01531.x

Thermodynamic Stability of Gadolinia-Doped Ceria Thin Film Electrolytes for Micro-Solid Oxide Fuel Cells

Jennifer L.M. Rupp,† Anna Infortuna, and Ludwig J. Gauckler

Nonmetallic Inorganic Materials, Department of Materials, Swiss Federal Institute of Technology, Zurich, Switzerland

Next-generation micro-solid oxide fuel cells for portable devices require nanocrystalline thin-film electrolytes in order to allow fuel cell fabrication on chips at a low operation temperature and with high power outputs. In this study, nanocrystalline gadolinia-doped ceria ($Ce_{0.8}Gd_{0.2}O_{1.9-x}$) thin-film electrolytes are fabricated and their electrical conductivity and thermodynamic stability are evaluated with respect to microstructure. Nanocrystalline gadolinia-doped ceria thin-film material ($Ce_{0.8}Gd_{0.2}O_{1.9-x}$) exhibits a larger amount of defects due to strain in the film than state-of-the-art microcrystalline bulk material. This strain in the film decreases the ionic conductivity of this ionic O^{2-} conductor. The thermodynamic stability of a nanocrystalline ceria solid solution with 65 nm grain size is reduced compared with microcrystalline material with 3–5 μm grain size. Nanocrystalline spray-pyrolyzed and PLD $Ce_{0.8}Gd_{0.2}O_{1.9-x}$ thin films with average grain sizes larger than 70 nm show predominantly ionic conductivity for temperatures lower than 700°C, which is high enough to be potentially used as electrolytes in low to intermediate-temperature micro-solid oxide fuel cells.

I. Introduction

GADOLINIA-DOPED ceria thin films have attracted considerable interest as electrolyte materials for solid oxide fuel cells (SOFCs) operating at intermediate temperatures.[1,2] The major advantages of SOFC with $Ce_{0.8}Gd_{0.2}O_{1.9-x}$ (CGO) electrolyte thin films are (i) the four to five times higher ionic conductivity at intermediate operating temperatures compared with state-of-the-art yttria-stabilized zirconia (YSZ),[2–4] (ii) the possibility to combine low-cost ceramic thin film methods like spray pyrolysis with traditional silicon micro-machining technologies for the production of micro-solid oxide fuel cells, and (iii) the reduced ohmic losses resulting in higher fuel cell power outputs.[5] One of the major disadvantages of microcrystalline CGO compared with YSZ is its mixed ionic-electronic conductivity, which becomes dominant especially for high fuel cell operating temperatures between 800° and 1000°C. In this temperature regime, electronic leakage through the fuel cell electrolyte leads to short circuiting and decreased power performance. However, if nanocrystalline CGO thin films are used, the ohmic resistance of the electrolyte, which scales linearly with its thickness, is drastically reduced and SOFC operation temperatures can be lowered to 500°–600°C. However, it is unclear whether these nanocrystalline thin films are as thermodynamically stable as standard microcrystalline-sintered CGO ceramics.

Spray pyrolysis[5,6] and pulsed laser deposition (PLD)[7] thin-film synthesis techniques allow the production of nanocrystalline SOFC electrolyte thin films with average grain sizes below 100 nm and film thicknesses between 100 and 500 nm. CGO spray-pyrolyzed and PLD thin films have dense microstructures after annealing for a short time at temperatures higher than 500°C and no further sintering steps are required.[8,9] It was reported in this recent study that the thin films exhibit a high amount of microstrain in the crystalline grains for average grain sizes below 100 nm. In electrical conductivity experiments measured in air, nanocrystalline CGO thin films prepared by spin coating, spray pyrolysis, and PLD exhibited a reduced oxygen vacancy mobility and a higher migration enthalpy with decreasing grain size and increasing microstrain.[10,11] The latter studies give the first indications that the electrical properties and thermodynamic stability might change in materials with high strain concentrations compared with strain-poor materials with micrometer grain size.

In the present investigation, we want to study the relation between ionic and electronic conductivity of CGO ceramics as a function of grain size, oxygen partial pressure, and temperature. The thermodynamic stability of CGO spray pyrolysis and PLD thin films with nano-sized grains is compared with that of a sintered bulk sample with grain sizes in the micrometer range.

II. Electric Conductivity of Gadolinia-Doped Ceria

Ceria-based materials are mixed ionic-electronic conductors transporting electrons via *n*-type small polaron hopping and oxygen ions via oxygen vacancies.[12,13] It depends on the doping level, temperature, and oxygen partial pressure of the surrounding gas phase whether gadolinia-doped ceria ceramics are mainly ionic or electronic conductors. At low oxygen partial pressures and elevated temperatures, the ceria becomes partially reduced, whereby oxygen vacancies and electrons are formed in order to maintain charge neutrality

$$2Ce_{Ce}^{x} + O_{O}^{x} \rightleftarrows 2Ce'_{Ce} + V_{O}^{\bullet\bullet} + \frac{1}{2}O_2 \tag{1}$$

Under these reducing conditions, ceria-based ceramics are predominantly electronic conductors. Additions of small gadolinia contents below 30 mol%[14,15] create additional oxygen vacancies, which can increase the overall ionic conductivity

$$Gd_2O_3 \rightleftarrows 2Gd'_{Ce} + V_{O}^{\bullet\bullet} + 3O_{O}^{x} \tag{2}$$

In oxygen partial pressure and temperature-dependent electrical conductivity measurements, information on the dominant conductivity type, ionic (σ_i) or electronic (σ_e), and the thermodynamic stability is provided. In general, the total conductivity (σ_{tot}) of gadolinia-doped ceria can be expressed by

$$\sigma_{tot} = \sigma_i + \sigma_e \tag{3}$$

The ionic conductivity is given as

$$\sigma_i(T) = (2q)\left[V_{O}^{\bullet\bullet}\right] v_i(T) = (2q)\left[V_{O}^{\bullet\bullet}\right] \frac{v_{0i}}{T} \exp\left(-\frac{\Delta H_m}{k_B T}\right) \tag{4}$$

T. Gur—contributing editor

Manuscript No. 22093. Received August 15, 2006; approved November 22, 2006.
Funding from BBW under contract number 03.0170-7 within the EU REAL–SOFC project is gratefully acknowledged
†Author to whom correspondence should be addressed. e-mail: jennifer.rupp@mat.ethz.ch

where T denotes the absolute temperature, $2q$ the charge of an oxygen vacancy, $[V_O^{\bullet\bullet}]$ their concentration, v_i the ionic mobility, v_{0i} the pre-exponential ionic mobility factor containing geometrical factors and the jump attempt frequency, ΔH_m the enthalpy of oxygen vacancy migration, and k_B the Boltzmann constant. Eq. (4) shows that only the ionic mobility is temperature dependent. The oxygen vacancy concentration of the ionic conductivity is neither temperature nor oxygen partial pressure dependent.[16,17]

The electronic conductivity of Eq. (3) is expressed as

$$\sigma_e(T) = e_0 n v_e(T) = e_0 n_0 \exp\left(-\frac{\Delta H}{k_B T}\right)\frac{v_{0e}}{T}\exp\left(-\frac{E_h}{k_B T}\right) \quad (5)$$

where e_0 denotes the electron charge, n their concentration, v_e the electronic mobility, n_0 the pre-exponential factor of electron concentration, ΔH the enthalpy of oxygen extraction, v_{0e} the pre-exponential electronic mobility factor, and E_h the electron hopping energy.[13,18] Concerning the electronic conductivity, it can be concluded that the electron mobility as well as the electron concentration depend on temperature. It is important to note in Eq. (5) that the formation of electrons during partial reduction of the ceria (Eq. (1)) is related to the formation of additional oxygen vacancies through the external reduction/oxidation equilibrium with the gas phase. The electronic conductivity is in contrast to the ionic conductivity oxygen partial pressure dependent

$$\sigma_e(T) \propto p(O_2)^{-\frac{1}{m}} \quad (6)$$

Only the electronic conductivity is affected by the present reduction/oxidation equilibrium and shows the oxygen partial pressure dependence; see Eq. (6). The ionic conductivity is in first approximation not affected by the reduction or oxidation of the ceria and remains oxygen partial pressure independent.

In case of gadolinia-doped ceria, a constant vacancy concentration n results in an oxygen partial pressure exponent $-1/m$ equal to $-1/4$. The oxygen partial pressure exponent decreases to $-1/m$ equal to $-1/6$ or in some cases even to $-1/10$ if the ceria is reduced and $[V_O] = n$ holds for the vacancy concentration. The defect model of trivalently doped ceria ceramics is described in further detail elsewhere.[2,19–21]

III. Experimental Procedure

(1) Spray Pyrolysis Thin-Film Preparation

The CGO spray pyrolysis precursor solutions were made of 0.02 mol/L gadolinium chloride (Alfa Aesar, 99.9% purity) and 0.08 mol/L cerium nitrate (Alfa Aesar, 99% purity) dissolved in 33:33:33 vol% ethanol, diethylene glycol monobutyl ether, and 1-methoxy-2-propanol (all solvents from Fluka Chemie, >99% purity). These precursor solutions were fed to a spray gun (Compact 2000KM, Bölhoff Verfahrenstechnik, Germany) at a liquid flow rate of 34.4 mL/h and atomized with 1.5 bar air pressure. The droplets produced in this manner were sprayed on a heated sapphire single-crystal substrate (Stettler, Switzerland) at 310 ± 10°C for 5 h, which was covered by a shadow mask to define the thin film geometry. By this spray pyrolysis, CGO thin films approximately 14 mm × 28 mm × 300–400 nm (length × width × film thickness) in size were produced on sapphire substrates. The working distance between the spray nozzle and the hot plate was maintained at 45 cm during all the experiments. The spray pyrolysis process is described in further detail elsewhere.[5,6,22]

(2) PLD Thin-Film Preparation

Pulsed laser-deposited CGO thin films were produced on sapphire substrates (Stettler, Switzerland) using a KrF excimer laser of 248 nm wavelength (Surface, Germany). The deposition was performed at 300°C, under vacuum, with 10 Hz laser pulsed frequency, 200 mJ energy per pulse, and at 60 mm target–substrate distance. During PLD, the target was ablated and the material was deposited through a shadow mask on a sapphire substrate. The dimension of final thin film on sapphire was approximately 14 mm × 28 mm × 500–800 nm (length × width × film thickness).

The PLD targets were produced by uniaxially (28 MPa for 3 min) and isostatically pressing (280 MPa for 3 min) CGO powder (Praxair, purity 99.9%). The pellets were heated up to 1400°C at 3°C/min, held at this temperature for 4 h, and cooled at 5°C/min to room temperature. The density of the pellets was evaluated using the Archimedes method and reached >98% of the theoretical value.

(3) Sintered Pellet Preparation

The CGO pellet green bodies were produced by first uniaxially pressing 4 g of CGO powder (Praxair, purity 99.9%) and subsequent isostatic pressing at 300 MPa for 3 min in a pressing form. Test bars of approximately 40 mm × 4 mm × 4 mm (length × width × height) were obtained and heated to 1500°C at 1°C/min, held there for 4 h, and cooled down at 5°C/min. to room temperature. The bars reached more than 99% of their theoretical density measured by the Archimedes method. For the microstructure investigations by scanning electron microscopy (SEM), the pellets were thermally etched at 1400°C for 20 min at 10°C/min. heating and cooling rates. After thermal etching, the samples were polished with SiC paper of decreasing roughness.

(4) Investigation of Microstructure

The thin-film microstructures were characterized using SEM Leo 1530, Germany). The average grain size was estimated from X-ray diffraction (XRD; Bruker AXS D8 Advance) data by means of the Scherrer equation for thin films with average grain sizes smaller than 80 nm.[23] Larger average grain sizes were characterized by measuring at least 300 grains in the SEM micrographs using the method of linear intercept with a grain intersection to grain size conversion factor of 1.56. For the average grain size evaluation, the program Lince 2.31 was used. The chemical composition was determined by energy-dispersive X-ray spectroscopy (EDX; Leo 1530, Zeiss Germany). For quantitative EDX analysis, the Proza correction method was chosen.

(5) Electrical Characterization

Electrical measurements were carried out for the sintered pellet, the spray pyrolyzed, and PLD thin films as a function of oxygen partial pressure and temperature. In Fig. 1, a schematic drawing of the electrical characterization setup is shown. The setup consists of a furnace with a gas-tight alumina tube in which an oxygen partial pressure in the range of 0.21 to 10^{-25} atm can be realized by flowing through the gas inlet O_2, air, air/N_2 mixtures, N_2, N_2/H_2 mixtures, or H_2, and controlling the gas flow by flow meters. The actual oxygen partial pressure was measured by the electromotive force (EMF) of a Y_2O_3-stabilized ZrO_2 sensor (EMF-sensor, see Fig. 1(4)), with one electrode exposed to air as a reference electrode and the second to the ambient oxygen partial pressure in the alumina tube. The EMF of the sensor was measured by a digital multimeter (175 A, Keithley).

For the electrical measurements, Pt electrodes (150 nm thickness, 1 mm width, and 14 mm length) were sputtered (SCD 050 Sputter Coater, Bal-Tec) on the thin-film samples through a shadow mask; see Fig. 2(a).

On each sputtered Pt electrode, a platinum wire was fixed to the substrate with platinum paste (C 3605 P, Heraeus GmbH) by two bonds of a ceramic two-component binder (Firag AG). The thin-film samples were heated to 300°C for 15 min to remove residual organics from the platinum paste. In the case of

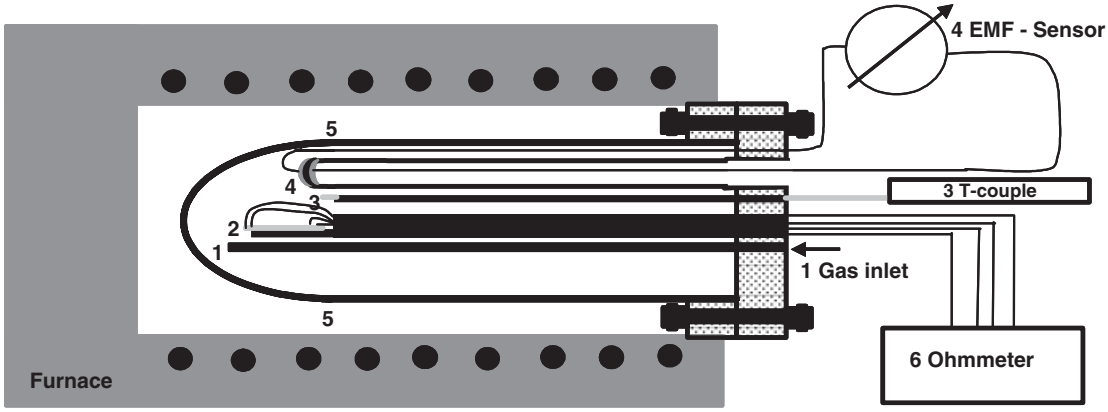

Fig. 1. Schematic setup for the four-point conductivity measurements as a function of temperature and oxygen partial pressure. 1, gas inlet, 2, sample on the sample holder, 3, thermocouple, 4, EMF-sensor, 5, alumina tube, and 6, Ohmmeter.

the sintered pellets, a Pt wire was wrapped around the sintered bar and Pt paste (C 3605 P, Heraeus GmbH) was used to improve the contact between the bar and the wires (see Fig. 2(b)). Afterwards, the organic of the platinum paste was burned out with the same heating program as used for the thin films. For the thin films, as well as for the bulk samples, four-point conductivity measurements were performed using a digital multimeter (197 A, Keithley).

The spray-pyrolyzed and the PLD thin films on sapphire substrates were both annealed for 10 h at 1000°C at a heating and cooling rate of 3°C/min. Thus, stable microstructures could be established for the electrical conductivity measurements, which were carried out between 500° and 900°C.

IV. Results and Discussion

(1) Microstructures and Chemical Analysis

The CGO microstructures are shown in the SEM plane views in Fig. 3 for a PLD (Fig. 3(a)) and a spray-pyrolyzed thin film (Fig. 3(b)) both after annealing at 1000°C for 10 h, and a sintered pellet sintered at 1500°C for 4 h (Fig. 3(c)). The PLD and spray-pyrolyzed thin films show dense and crack-free microstructures with average grain sizes of 65 and 78 nm, respectively. For both thin films, the film thickness was around 400 nm. The microstructure of the sintered CGO pellet (Fig. 3(c)) is >99% dense with an average grain size of 3.51 μm. In Table I, the determined average grain sizes for PLD and spray pyrolysis thin films as well as for the sintered pellet are summarized.

The chemical compositions of the sintered pellet, the spray-pyrolyzed, and PLD films were analyzed by EDX using the cerium and gadolinium L lines for the quantitative analysis. The EDX analysis revealed 22±2 cat% (spray pyrolysis), 25±1 cat% (PLD), and 20±2 cat% (sintered pellet) of gadolinia in the ceria lattice. The XRD patterns of all specimens investigated here have the cubic face-centered crystal structure of CGO with a lattice constant of 0.541±0.001 nm, which is in good agreement with other literature data.[24–27]

(2) Electrical Characterization

In Fig. 4, the total conductivities (σ) for a PLD thin film (Fig. 4(a)), a spray-pyrolyzed thin film (Fig. 4(b)), and a sintered pellet (Fig. 4(c)) are plotted as a function of oxygen partial pressure (pO_2) and temperature.

All samples show mixed ionic electronic conductivity behavior with the following characteristics: (i) At high and intermediate pO_2, the total conductivity is independent of pO_2 and ionic conductivity prevails. (ii) For low pO_2, the total conductivity depends on the pO_2 and *n*-type electronic conductivity (σ_e) with $\sigma_e \propto pO_2^{-1/m}$ being present. The pO_2 exponents of the thin films equal mostly −1/4 for 500°–900°C, but a transition from $-1/m = -1/4$ to $-1/m = -1/6$ can be observed at pO_2 lower than 10^{-21} atm and for temperatures higher than 800°C for PLD films (Fig. 4(a)) and at pO_2 lower than 10^{-17} atm and temperatures higher than 900°C for spray-pyrolyzed films (Fig. 4(b)). Schneider *et al.*[19] observed in coulometric titration experiments a transition of the pO_2 exponent from −1/4 to −1/6 for pO_2 below 10^{-18} and 900°C for microcrystalline CGO. In defect model calculations, the authors acknowledged that at low nonstoichiometries, the defect interactions are small and therefore the slope of the electronic conductivity approaches −1/4, and that at larger nonstoichiometries, coupling between the increasing concentrations of oxygen vacancies and electrons changes the slope to 1/6. The PLD thin films show large nonstoichiometry already at 800°C, characterized by the transition of the pO_2

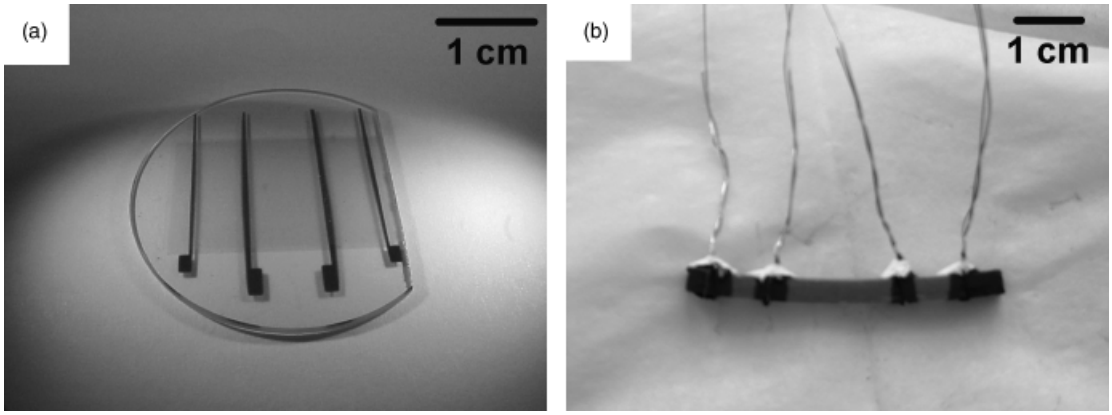

Fig. 2. 4-point conductivity specimens: (a) $Ce_{0.8}Gd_{0.2}O_{1.9-x}$ (CGO) spray pyrolysis thin film and (b) CGO bulk sample.

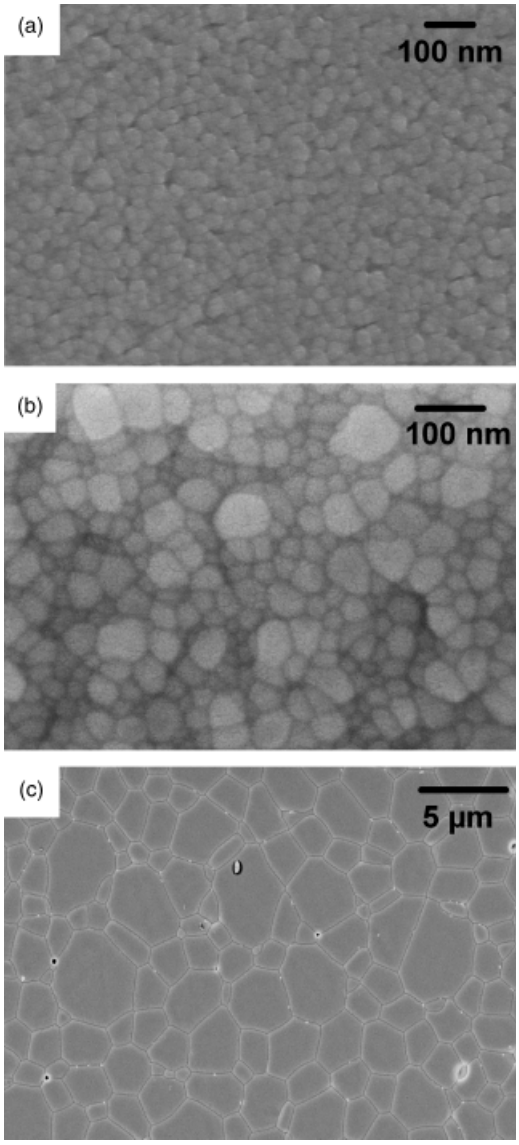

Fig. 3. Microstructures of $Ce_{0.8}Gd_{0.2}O_{1.9-x}$ (a) pulsed laser deposition thin film, (b) spray pyrolysis thin film and (c) sintered pellet.

exponent from $-1/4$ to $-1/6$, whereas the larger grain-sized spray pyrolysis thin films or microcrystalline samples[19] show this transition first at a 100°C higher temperature. (iii) The point where the ionic and electronic conductivity are equal is the so-called electrolytic domain boundary (EDB). With decreasing temperature, the EDB shifts to a lower pO_2 and ionic conductivity becomes more dominant compared with the electronic.

In Fig. 5, the Arrhenius plot of the EDB with respect to temperature is displayed for the sintered pellet, the spray-pyrolyzed, and the PLD thin films. The pO_2 of the EDB for the thin films is about four decades higher at all temperatures compared with the

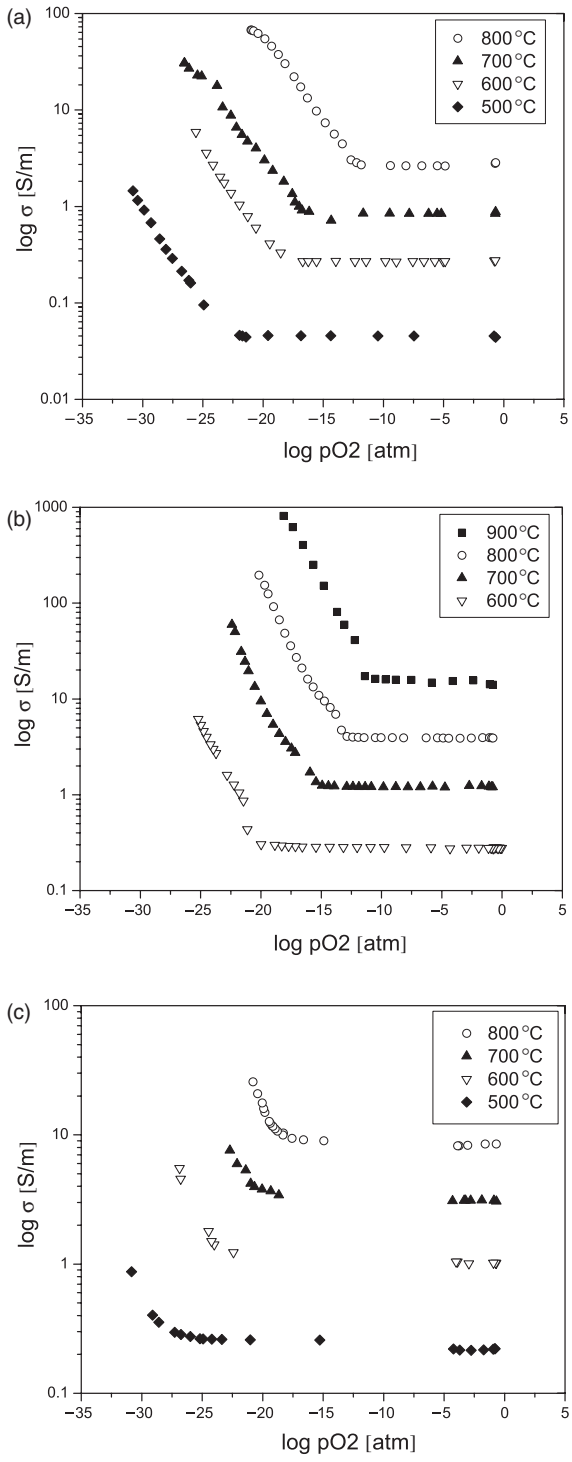

Fig. 4. Total conductivity (σ) versus oxygen partial pressure (pO_2) and temperature for $Ce_{0.8}Gd_{0.2}O_{1.9-x}$ (a) pulsed laser deposition thin film, (b) spray pyrolysis thin film, and (c) sintered pellet.

Table I. Average Grain Size, Ionic Conductivity (σ_i and its Activation Energy (E_a)), and Electrolytic Domain Boundary (EDB) and Its Activation Energy for $Ce_{0.8}Gd_{0.2}O_{1.9-x}$ Pulsed Laser Deposition (PLD) Thin Films, Spray Pyrolysis Thin Films, and Sintered Pellets

Preparation method of $Ce_{0.8}Gd_{0.2}O_{1.9-x}$	Average grain size	σ_i (S/m) at 500°C	σ_i (S/m) at 700°C	E_a (eV) of σ_i	EDB (atm.) at 700°C	E_a (eV) of EDB (atm.)
PLD thin film	65 nm	0.05	0.80	0.98	1.74×10^{-17}	5.13
Spray pyrolysis thin film	78 nm	0.09	2.45	0.97	3.79×10^{-16}	5.13
Sintered pellet	3.51 μm	0.25	0.98	0.78 ($400°C > T$) 0.90 ($T < 400°C$)	6.96×10^{-21}	5.14

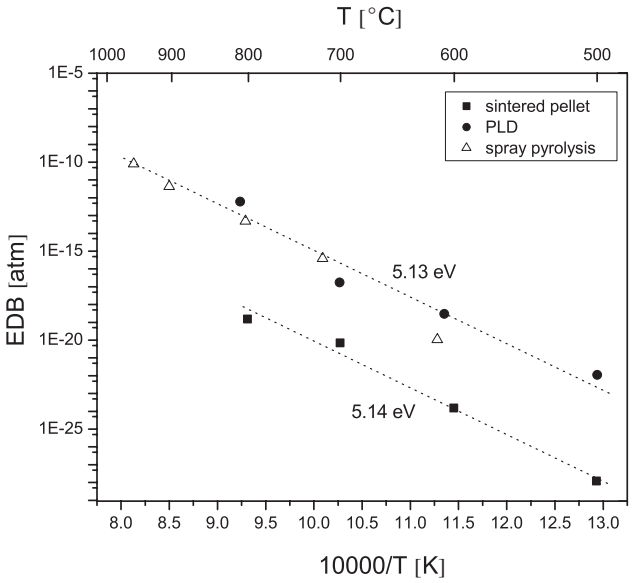

Fig. 5. Arrhenius plot of the electrolytic domain boundary (EDB) of $Ce_{0.8}Gd_{0.2}O_{1.9-x}$ pulsed laser deposition thin films, spray pyrolysis thin films, and sintered pellets.

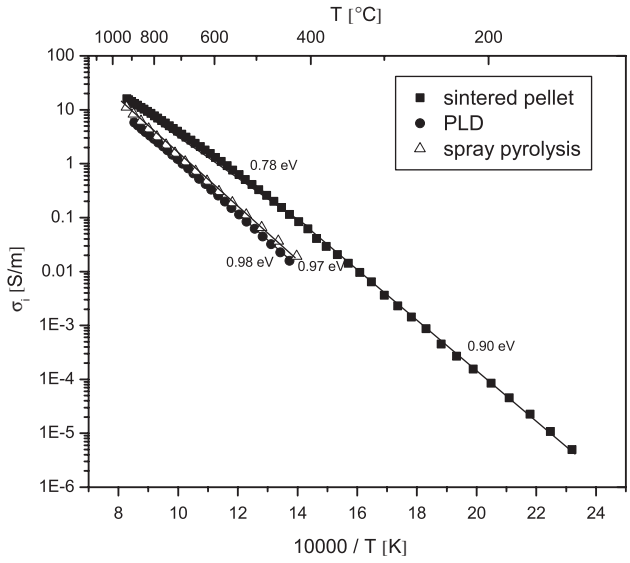

Fig. 7. Ionic conductivity (σ_i of $Ce_{0.8}Gd_{0.2}O_{1.9-x}$) for pulsed laser deposition thin films, spray pyrolysis thin films, and sintered pellets, as a function of temperature (T) measured in air.

CGO bulk sample measured here or any other microcrystalline CGO sample reported in the literature.[3,19] The activation energies of the EDB for the small-grained thin film samples and the microcrystalline-sintered pellet are nearly equal, with 5.13 and 5.14 eV, respectively.

In Fig. 6, the pO_2 of the EDB at 700°C is plotted versus the average grain size for the samples of this study and the values from the literature of CGO spin-coated thin films[16] and sintered pellets.[3,19] With decreasing average grain size of the sample, the pO_2 of the EDB at 700°C shifts toward higher pO_2. With decreasing average grain size the CGO is more easily reduced and shows electronic conductivity over a wide pO_2 range. As the activation energy of the EDB is almost equal for the small grain-sized thin-film samples and the microcrystalline sintered pellet (Fig. 5), the nanocrystalline CGO thin films become reduced at higher pO_2 than a microcrystalline sample in the temperature range from 500° to 900°C.

Consequently, nanocrystalline CGO thin-film electrolytes should be operated at temperatures below 700°C to be primarily ionic conductors in SOFCs. In electrical conductivity experiments of undoped CeO_{2-x}[18] as a function of average grain size, observations similar to ours were made on CGO (Fig. 6): For microstructures with average grain sizes (d) below 300 nm, CeO_2 and CGO show an increased electronic and decreased ionic conductivity in which the scaling law $EDB \propto d^{-5.5}$ holds.

Experiments of microstrain evolution in the crystalline grains[8] and the influence of microstrain on electrical conductivity[11] in nanocrystalline CGO thin films showed that samples annealed at low temperatures with a small average grain size exhibited a large amount of defects and microstrain in the crystal lattice. If large average grain sizes were established and crystallization proceeded, the concentration of defects in the crystalline grains decreased rapidly.

The increased electronic conductivity and nonstoichiometry of CGO with decreased grain size (Fig. 6) for grains smaller than 300 nm is experimentally observed as a "grain size effect" in this study. It is reasonable to assume that the increased amount of additional defects (microstrain) in the crystal lattice results in changes in the thermodynamic properties while decreasing the grain size.

In Fig. 7, the ionic conductivities of the nanocrystalline PLD and spray-pyrolyzed thin films (measured in air) are compared with that of the microcrystalline-sintered pellet. The ionic conductivity of the spray pyrolyzed thin film is slightly higher than for the PLD film, but both nanocrystalline materials show a two to three times lower ionic conductivity than the sintered pellet with micro-sized grains and other literature references on sintered pellets.[3,24,25,28] In Table I, the ionic conductivities measured at 500° and 700°C and their activation energies are summarized. The fact that the ionic conductivity in air of the nanocrystalline thin films is decreased compared with the microcrystalline samples agrees with the results previously shown in Figs. 4 and 6.

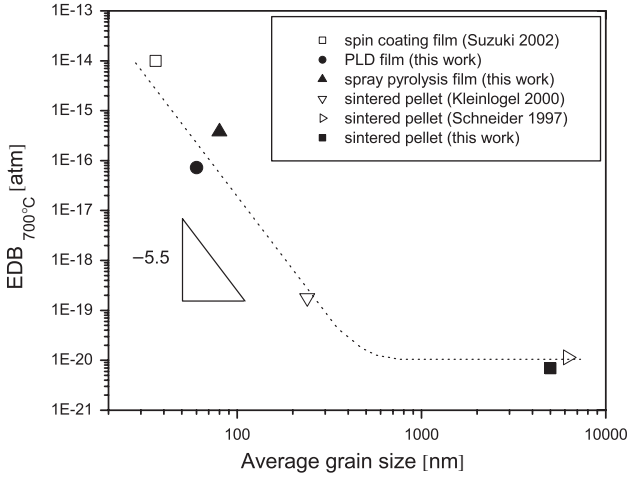

Fig. 6. Electrolytic domain boundary (EDB) at 700°C of $Ce_{0.8}Gd_{0.2}O_{1.9-x}$ for pulsed laser deposition thin films, spray pyrolysis thin films, and sintered pellets, as a function of average grain size.

V. Conclusions

The oxygen vacancy migration and the electronic conductivity of gadolinia-doped ceria solid solutions are heavily dependent on the microstructure for average grain sizes smaller than roughly 300 nm. The ionic conductivity decreases and the electronic conductivity increases with decreasing average grain size and increasing amount of defects in the microstructure. The electrolytic domain boundary of CGO with an average grain size of 65 nm occurs at higher pO_2 ($+\Delta p_{O2} = 10^{-4}$ atm) compared with microcrystalline material for 500° to 800°C.

For average grain sizes around 70 nm, PLD and spray-pyrolyzed thin films show similar ionic conductivities between 0.8

and 0.98 S/m at 700°C, which are by a factor of two to three lower than microcrystalline CGO. However, this reduced ionic conductivity is less important, considering the reduction of ohmic losses using an electrolyte thin film with roughly 300 nm thickness that has a 100 times lower ohmic resistance than any other state-of-the-art microcrystalline CGO electrolyte with thickness in the 10–200 μm range.

Micro-solid oxide fuel cell operation with nanocrystalline gadolinia-doped ceria spray pyrolysis or PLD thin films as electrolyte material might be feasible if the cell is operated at low temperatures 500°–600°C and the grains are kept as large as possible.

References

[1]I. Taniguchi, R. C. van Landschoot, and J. Schoonman, "Electrostatic Spray Deposition of $Gd_{0.1}Ce_{0.9}O_{1.95}$ and $La_{0.9}Sr_{0.1}Ga_{0.8}Mg_{0.2}O_{2.87}$ Thin Films," *Solid State Ionics*, **160**, 271 (2003).

[2]M. Mogensen, N. M. Sammes, and G. A. Tompsett, "Physical, Chemical and Electrochemical Properties of Pure and Doped Ceria," *Solid State Ionics*, **129**, 63 (2000).

[3]C. Kleinlogel and L. J. Gauckler, "Sintering and Properties of Nanosized Ceria Solid Solutions," *Solid State Ionics*, **135**, 567 (2000).

[4]M. Gödickemeier, K. Sasaki, and L. J. Gauckler, "Electrochemical Characteristics of Cathodes in Solid Oxide Fuel Cells Based on Ceria Electrolytes," *J. Electrochem. Soc.*, **144**, 1635 (1997).

[5]D. Perednis and L. J. Gauckler, "Solid Oxide Fuel Cells With Electrolytes Prepared Via Spray Pyrolysis," *Solid State Ionics*, **166**, 229 (2004).

[6]D. Perednis, O. Wilhelm, S. E. Pratsinis, and L. J. Gauckler, "Morphology and Deposition of Thin Yttria-Stabilized Zirconia Films Using Spray Pyrolysis," *Thin Solid Films*, **474**, 84 (2005).

[7]J. Will, A. Mitterdorfer, C. Kleinlogel, D. Perednis, and L. J. Gauckler, "Fabrication of Thin Electrolytes for Second-Generation Solid Oxide Fuel Cells," *Solid State Ionics*, **131**, 79 (2000).

[8]J. L. M. Rupp, A. Infortuna, and L. J. Gauckler, "Microstrain and Self-Limited Grain Growth in Nanocrystalline Ceria Ceramics," *Acta Materialia*, **54**, 1721 (2006).

[9]J. L. M. Rupp, C. Solenthaler, P. Gasser, U. P. Muecke, and L. J. Gauckler, "Crystallization of Ceria Solid Solutions from the Amorphous Phase," *Acta Materialia*, 2006, in press.

[10]I. Kosacki, T. Suzuki, H. U. Anderson, and P. Colomban, "Raman Scattering and Lattice Defects in Nanocrystalline CeO_2 Thin Films," *Solid State Ionics*, **149**, 99 (2002).

[11]J. L. M. Rupp and L. J. Gauckler, "Microstructures and Electrical Conductivity of Nanocrystalline Ceria based Thin Films," *Solid State Ionics*, **177** [26-32], 2513–8 (2006).

[12]H. L. Tuller, "Semiconduction and Mixed Ionic-Electronic Conduction in Nonstoichiometric Oxides: Impact and Control," *Solid State Ionics*, **94**, 63 (1997).

[13]H. L. Tuller and A. S. Nowick, "Small Polaron Electron Transport in Reduced CeO_2 Single Crystals," *J. Phys. Chem. Solids*, **38**, 859 (1977).

[14]Z. Tianshu, P. Hing, H. Huang, and J. Kilner, "Onic Conductivity in the CeO_2-Gd_2O_3 System ($0.05 <= Gd/Ce <= 0.4$) Prepared by Oxalate Coprecipitation," *Solid State Ionics*, **148**, 567 (2002).

[15]B. C. H. Steele, "Appraisal of Ce1-*y*GdyO2-*y*/2 Electrolytes for IT-SOFC Operation at 500°C," *Solid State Ionics*, **129**, 95 (2000).

[16]T. Suzuki, I. Kosacki, and H. U. Anderson, "Microstructure-Electrical Conductivity Relationships in Nanocrystalline Ceria Thin Films," *Solid State Ionics*, **151**, 111 (2002).

[17]T. Suzuki, I. Kosacki, H. U. Anderson, and P. Colomban, "Electrical Conductivity and Lattice Defects in Nanocrystalline Cerium Oxide Thin Films," *J. Amer. Ceram. Soc.*, **84**, 2007 (2001).

[18]A. Tschope and R. Birringer, "Grain size Dependence of Electrical Conductivity in Polycrystalline Cerium Oxide," *J. Electroceram.*, **7**, 169 (2001).

[19]D. Schneider, M. Godickemeier, and L. J. Gauckler, "Nonstoichiometry and Defect Chemistry of Ceria Solid Solutions," *J. Electroceram.*, **1**, 165 (1997).

[20]G. M. Christie and F. P. F. van Berkel, "Microstructure—Ionic Conductivity Relationships in Ceria-Gadolinia Electrolytes," *Solid State Ionics*, **83**, 17 (1996).

[21]J. C. C. Abrantes, D. Perez-Coll, P. Nunez, and J. R. Frade, "Electronic Transport in Ce0.8Sm0.2O1.9-[delta] Ceramics Under Reducing Conditions," *Electrochim. Acta*, **48**, 2761 (2003).

[22]P. S. Patil, "Versatility of Chemical Spray Pyrolysis Technique," *Mater. Chem. Phys.*, **59**, 185 (1999).

[23]P. Scherrer, "Bestimmung der Grösse und der inneren Struktur von Kolloidteilchen mittels Röntgenstrahlen," *Nachrichten von der Königlichen Gesellschaft der Wissenschaft zu Göttingen: Mathematisch-physikalische Klasse*, **1**, 98 (1918).

[24]S. Dikmen, P. Shuk, M. Greenblatt, and H. Gocmez, "Hydrothermal Synthesis and Properties of Ce1-*x*GdxO2-[delta] Solid Solutions," *Solid State Sci.*, **4**, 585 (2002).

[25]G. S. Lewis, A. Atkinson, B. C. H. Steele, and J. Drennan, "Effect of Co Addition on the Lattice Parameter, Electrical Conductivity and Sintering of Gadolinia-Doped Ceria," *Solid State Ionics*, **153**, 567 (2002).

[26]J. Ma, T. S. Zhang, L. B. Kong, P. Hing, and S. H. Chan, "Ce0.8Gd0.2O2-[delta] Ceramics Derived from Commercial Submicron-Sized CeO_2 and Gd_2O_3 Powders for Use as Electrolytes in Solid Oxide Fuel Cells," *J. Power Sources*, **132**, 71 (2004).

[27]H. Z. Song, H. B. Wang, S. W. Zha, D. K. Peng, and G. Y. Meng, "Aerosol-Assisted MOCVD Growth of Gd_2O_3-Doped CeO_2 Thin SOFC Electrolyte Film on Anode Substrate," *Solid State Ionics*, **156**, 249 (2003).

[28]E. Jud, C. B. Huwiler, and L. J. Gauckler, "The Effect of Cobalt Oxide Addition on the Conductivity of Ce0.8Gd0.2O1.9," *J. Electroceram.*, **15**, 159 (2005). □